Available online at www.sciencedirect.com
ScienceDirect
Trans. Nonferrous Met. Soc. China 35(2025) 2049−2060
Transactions of Nonferrous Metals Society of China
www.tnmsc.cn

# Transformation behavior of calcium vanadate and manganese vanadate in $CaO−V_2O_5−MnO_2$ system during calcification roasting of vanadium slag

Jing WEN[1], Tao JIANG[1,2,3], Fei-fei LI[1], Tang-xia YU[1], Bo-jian CHEN[1]

1. School of Metallurgy, Northeastern University, Shenyang 110819, China;
2. Key Laboratory for Ecological Metallurgy of Multimetallic Mineral (Ministry of Education), Northeastern University, Shenyang 110819, China;
3. Liaoning Key Laboratory for Metallurgical Sensor and Technology, Shenyang 110819, China

Received 13 October 2023; accepted 19 July 2024

**Abstract:** A simplified $CaO−V_2O_5−MnO_2$ system was established to qualitatively and quantitatively investigate the transformation behavior of vanadates. The results demonstrated dynamic transformations between calcium vanadate and manganese vanadate as $n(CaO)/n(V_2O_5)/n(MnO_2)$ ratios and roasting temperatures varied. When $MnO_2$ was incrementally added with $n(CaO)/n(V_2O_5)$ of 2, some $Ca_2V_2O_7$ converted to $Mn_2V_2O_7$. The mass of vanadium as calcium vanadate consistently exceeded that as manganese vanadate. Conversely, when CaO was gradually added with $n(MnO_2)/n(V_2O_5)$ of 2, $Mn_2V_2O_7$ tended to transform into $Ca_2V_2O_7$ and $Ca_3V_2O_8$. The affinity of vanadium for calcium was higher compared that of vanadium for manganese. The specific type of calcium vanadate formed depended on both $n(CaO)/n(V_2O_5)/n(MnO_2)$ values and roasting temperatures, while manganese vanadate remained predominantly as $Mn_2V_2O_7$. The influence of roasting temperature on the conversion between calcium vanadate and manganese vanadate was minimal. At $n(CaO)/n(V_2O_5)/n(MnO_2)$ of 2/1/2 and temperatures ranging from 650 to 850 °C, the mass ratio of vanadium present as calcium vanadate to manganese vanadate stabilized at approximately 2.

**Key words:** transformation behavior; $CaO−V_2O_5−MnO_2$; calcium vanadate; manganese vanadate; vanadium slag; calcification roasting

## 1 Introduction

Vanadium and its compounds are extensively utilized in metallurgy, chemicals, aerospace, and other industries, playing a crucial role in China's national economic development [1−4]. Notably, in the context of "carbon peaking and carbon neutrality," the demand for vanadium in China has surged because of the increasing use of V−N microalloyed steel and all-vanadium liquid flow batteries [5−10].

Vanadium−titanium magnetite is currently the primary raw material for vanadium extraction, accounting for over 88% of global vanadium supply [11−14]. Additionally, stone coal and spent catalysts serve as alternative sources for vanadium extraction [15−19]. The Panzhihua−Xichang area in Sichuan and the Chengde area in Hebei province are abundant in vanadium−titanium magnetite. In these regions, blast furnace ironmaking and converter blowing are employed to concentrate vanadium into vanadium slag, a critical byproduct material for vanadium extraction in China [20,21].

In recent decades, numerous effective technologies for vanadium extraction from vanadium slag have been developed by enterprises and research institutes [22−27]. The sodium salt roasting−

**Corresponding author:** Tao JIANG, Tel: +86-24-83687324, E-mail: jiangt@smm.neu.edu.cn
https://doi.org/10.1016/S1003-6326(25)66800-2

water leaching process and the calcification roasting−acid leaching process have been industrialized, both relying on roasting techniques [28−31]. Non-roasted processes, such as those involving sub-molten salts and chlorination, have also been proposed [32,33]. Among these methods, the calcification roasting−acid leaching process demonstrates significant economic, environmental, and efficiency advantages, positioning it as a highly promising vanadium extraction method. Consequently, a production line with an annual output of 20000 t of $V_2O_5$ has been established at Xichang Steel Vanadium Co., Ltd., Sichuan, China [34]. Our group has conducted extensive research and process optimization on the calcification roasting of vanadium slag and chromium-containing vanadium slag [14,35].

Our investigations revealed that, during the calcification roasting process, vanadium not only reacts with calcium additives to form calcium vanadate but also inevitably reacts with the manganese components in vanadium slag to produce manganese vanadate [21]. This discovery led to the innovative proposal of a manganese roasting process for vanadium extraction [24,36,37]. During this process, the original calcium component in vanadium slag participated in the conversion of vanadium spinel to vanadate. These findings indicate that both calcium and manganese salts exhibit high reactivity with vanadium. However, the reaction mechanisms of vanadium with calcium and manganese, as well as the generation and conversion behavior of calcium vanadate and manganese vanadate, remain underexplored. These insights are critical for optimizing vanadium extraction through calcification roasting from vanadium slag and chromium-containing vanadium slag.

To address the interference of original components in vanadium slag, such as iron, chromium, titanium, and silicon, in studying the interactions among calcium, manganese, and vanadium, $V_2O_5$ was used to simplify the vanadium spinel in vanadium slag. CaO and $MnO_2$ were employed as the simplest calcium and manganese additives, respectively. A $CaO−V_2O_5−MnO_2$ three-phase system was established to investigate the phase evolution of calcium vanadate and manganese vanadate by varying the molar ratio and roasting temperature. Finally, the distribution of vanadium in calcium vanadate and manganese vanadate was quantitatively analyzed via acid leaching.

## 2 Experimental

### 2.1 Materials

Vanadium exists as $(Mn,Fe)(V,Cr)_2O_4$ in both vanadium slag and chromium-containing vanadium slag [38,39], which oxidizes to high-valence vanadium oxide during roasting. Therefore, $V_2O_5$ was used as the raw material for the roasting process with CaO and $MnO_2$ in this study. The three oxides were analytical-grade reagents sourced from Sinopharm Chemical Reagent Co., Ltd. CaO was roasted at 1000 °C for 2 h to ensure the removal of $Ca(OH)_2$ and $CaCO_3$, thereby improving the precision of the mixing process. Figure 1 presents the XRD patterns of $V_2O_5$, CaO, and $MnO_2$. The diffraction peaks of these three raw materials are well indexed to those of the Joint Committee on Powder Diffraction Standards, which meet the requirements for the mixing and roasting process.

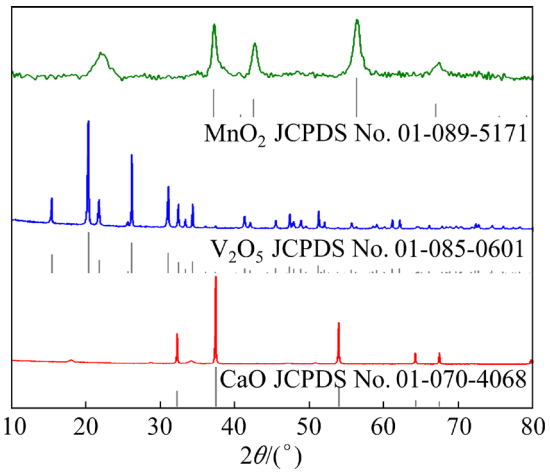


**Fig. 1** XRD patterns of $V_2O_5$, CaO and $MnO_2$

### 2.2 Design of $CaO−V_2O_5−MnO_2$ system

$V_2O_5$, CaO and $MnO_2$ were mixed uniformly to establish the $CaO−V_2O_5−MnO_2$ three-phase system. The mixing ratio was calculated based on their molar ratios and expressed as $n(CaO)/n(V_2O_5)/n(MnO_2)$. Three experimental groups were designed by varying the quantities of the components. First, the amounts of $V_2O_5$ and CaO were fixed, and $MnO_2$ was gradually added to study

the transformation mechanism from calcium vanadate to manganese vanadate. A $n(CaO)/n(V_2O_5)$ ratio of 2 was selected for mixing $V_2O_5$ and CaO, as the target phase calcium pyrovanadate ($Ca_2V_2O_7$) forms during the calcification roasting process of actual vanadium slag and chromium-containing vanadium slag [14]. $MnO_2$ was added at $n(MnO_2)/n(V_2O_5)$ ratios of 1, 2 and 3. Additionally, a two-phase system containing only $V_2O_5$ and CaO was studied for comparison.

Second, the amounts of $V_2O_5$ and $MnO_2$ were fixed with a $n(MnO_2)/n(V_2O_5)$ ratio of 2, generating the target product manganese pyrovanadate ($Mn_2V_2O_7$) during the manganese roasting of actual vanadium slag and chromium-containing vanadium slag [37]. CaO was gradually added to study the transformation mechanism from manganese vanadate to calcium vanadate with $n(CaO)/n(V_2O_5)$ ratios of 1, 2 and 3. A two-phase system containing $V_2O_5$ and $MnO_2$ was also analyzed as a control.

Third, the mass of $V_2O_5$ in the system was kept constant to investigate the competitive behavior of CaO and $MnO_2$ in reacting with vanadium quantitatively. Furthermore, $n(CaO)/n(V_2O_5)$ and $n(MnO_2)/n(V_2O_5)$ were set to the same values, ranging from 0.5 to 3. All experimental points are indicated in Fig. 2.

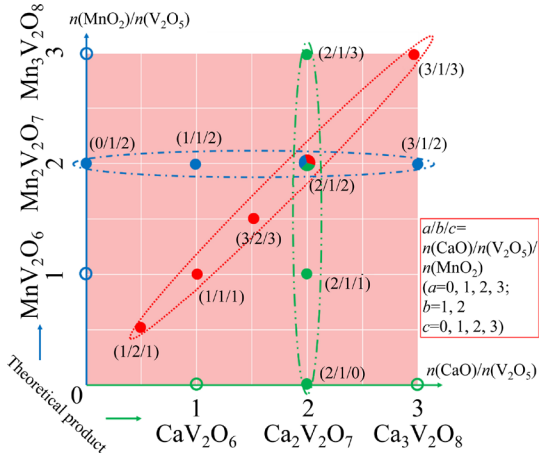


**Fig. 2** Experimental points in this work

### 2.3 Roasting of $CaO−V_2O_5−MnO_2$ system

In examining the effects of $n(CaO)/n(V_2O_5)/n(MnO_2)$ on phase evolution, the mixed materials were roasted from room temperature to 850 °C at a heating rate of 5 °C/min, reflecting the calcification and manganese roasting conditions of vanadium slag and chromium-containing vanadium slag [20,36]. A constant-temperature roasting process was conducted at 850 °C for 2 h to ensure complete reaction progress. The roasted samples were then cooled in the muffle furnace and ground for characterization. Additionally, the effect of roasting temperature was studied, ranging from 350 to 950 °C. The mixed samples with a $n(CaO)/n(V_2O_5)/n(MnO_2)$ ratio of 2/1/2 were selected for studying the effect of roasting temperature due to their uniqueness in Fig. 2. Other roasting conditions, such as heating rate and holding time, were kept constant.

### 2.4 Calculation of distribution behavior of vanadium

Leaching experiments were conducted to evaluate the amount of vanadium reacting with calcium and manganese, and clarify the conversion mechanism of calcium vanadate and manganese vanadate under different conditions. Approximately 99% of $Mn_2V_2O_7$ can be dissolved by $H_2SO_4$ solution with pH of 2.2, while high-valence manganese oxides ($MnO_2$, $Mn_3O_4$, and $Mn_2O_3$) are barely soluble under these conditions [24]. Hence, $H_2SO_4$ with pH of 2.2 was used as the leaching medium to dissolve the roasted materials of the $CaO−V_2O_5−MnO_2$ system. The total mass of vanadium in the system was calculated based on the amount of $V_2O_5$ added, and the mass of vanadium reacting with manganese was determined from the manganese concentration in the leaching solution. The mass of vanadium reacting with calcium was obtained by subtracting the mass of vanadium reacting with manganese from the total mass of vanadium.

### 2.5 Characterization

X-ray diffractometer (X Pertpro, PANalytical B.V.) was used to detect the phases of the experimental raw materials and roasted materials. SEM (Ultra plus, Zeiss, Germany) equipped with an EDS spectrometer was employed for analyzing the microstructure and elements distribution of the main elements in the roasted materials. Vanadium content in the vanadium-containing leaching solution was detected by ferrous ammonium sulfate titration method. Concentration of manganese in the leaching solution was detected with inductively coupled plasma–atomic emission spectroscopy (ICP–AES, PerkinElmer Optima−4300DV).

## 3 Results and discussion

### 3.1 Phase evolution of $CaO-V_2O_5$ and $MnO_2-V_2O_5$ system

The two-phase systems of $CaO-V_2O_5$ and $MnO_2-V_2O_5$ were roasted to establish a baseline before examining the mixtures of $V_2O_5$, CaO, and $MnO_2$. The theoretical molar ratios $n(CaO)/n(V_2O_5)$ of 1, 2 and 3 correspond to the formation of calcium metavanadate ($CaV_2O_6$), calcium pyro-vanadate ($Ca_2V_2O_7$), and calcium orthovanadate ($Ca_3V_2O_8$), respectively. Similarly, $n(MnO_2)/n(V_2O_5)$ ratios of 1, 2 and 3 theoretically produce manganese metavanadate ($MnV_2O_6$), manganese pyrovanadate ($Mn_2V_2O_7$), and manganese orthovanadate ($Mn_3V_2O_8$). Figures 3 and 4 present the XRD patterns, microstructures, and EDS analyses of the roasted samples with varying $n(CaO)/n(V_2O_5)$ and $n(MnO_2)/n(V_2O_5)$ ratios.

As illustrated in Fig. 3, when $n(CaO)/n(V_2O_5)$ was 1 and 2, the diffraction peaks of CaO and $V_2O_5$ disappeared, indicating the formation of $CaV_2O_6$ and $Ca_2V_2O_7$, respectively, as confirmed by their corresponding standard diffraction cards. However, at a ratio of 3, the diffraction peaks of CaO (at 32.23°, 37.38°, and 53.90°) and $Ca_2V_2O_7$ (at 28.72° and 29.97°) were still present alongside those of the target product $Ca_3V_2O_8$, suggesting incomplete calcification of $Ca_2V_2O_7$ to $Ca_3V_2O_8$. Figures 3(b−d) show the microstructures of the products roasted with different $n(CaO)/n(V_2O_5)$ ratios, with EDS analyses of various particles provided in Figs. 3(e−i). These particles exhibited irregular block structures. The atomic ratios of vanadium to calcium at Points *A* and *B* were close to 2 and 1, consistent with the theoretical values for $CaV_2O_6$ and $Ca_2V_2O_7$, respectively. The smaller particles in Fig. 3(d) represented unreacted CaO, confirmed by the element composition at Point *C*. Moreover, the coexistence of $Ca_2V_2O_7$ and $Ca_3V_2O_8$ was demonstrated by the atomic ratios of vanadium to calcium at Points *D* and *E*. The generation reaction equations for $CaV_2O_6$, $Ca_2V_2O_7$, and $Ca_3V_2O_8$ are depicted in Eqs. (1) to (3).

Figure 4 illustrates the XRD patterns, microstructures, and EDS analyses of the roasted samples with different $n(MnO_2)/n(V_2O_5)$ ratios. As depicted in Fig. 4(a), $MnV_2O_6$ and $Mn_2V_2O_7$ formed when $n(MnO_2)/n(V_2O_5)$ was 1 and 2, respectively, as evidenced by the consistency between the diffraction peaks and standard cards, along with the EDS analyses of Points *A* and *B*. These samples exhibited rough and smooth regular block particles. When $n(MnO_2)/n(V_2O_5)$ was 3, $Mn_3V_2O_8$ did not form; instead, $Mn_2V_2O_7$ and $Mn_2O_3$ were produced, indicating the difficulty of obtaining $Mn_3V_2O_8$ under the given roasting

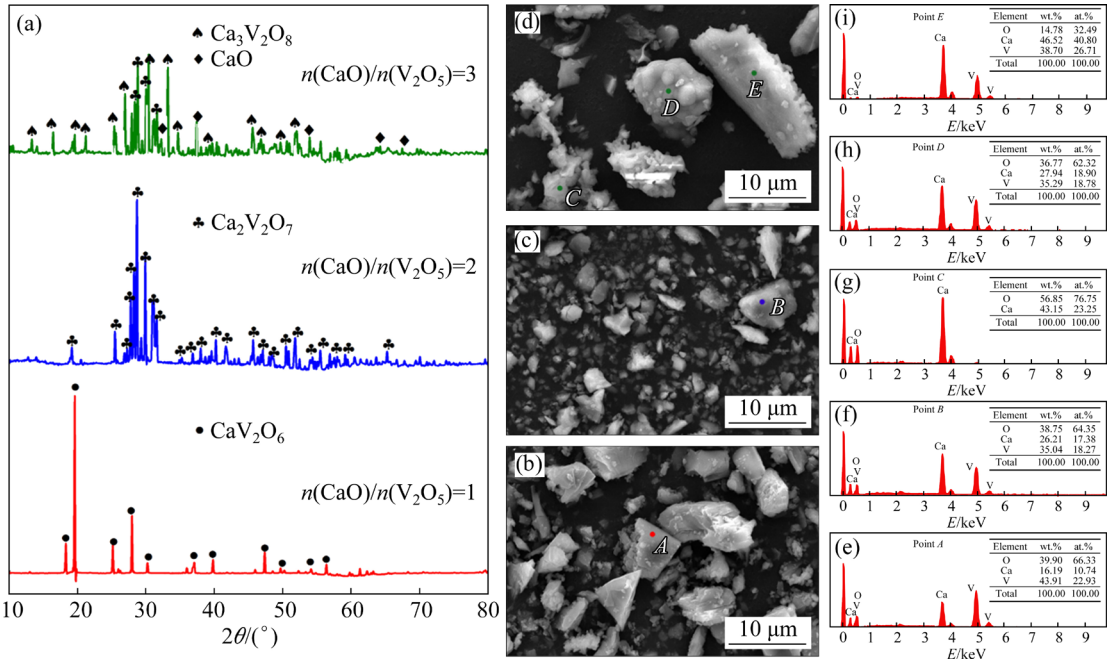


**Fig. 3** XRD patterns (a) and microstructures (b−d) of roasted samples of $CaO-V_2O_5$ system with different $n(CaO)/n(V_2O_5)$ ratios, and corresponding EDS analysis results (e−i): (b) Ratio of 1; (c) Ratio of 2; (d) Ratio of 3

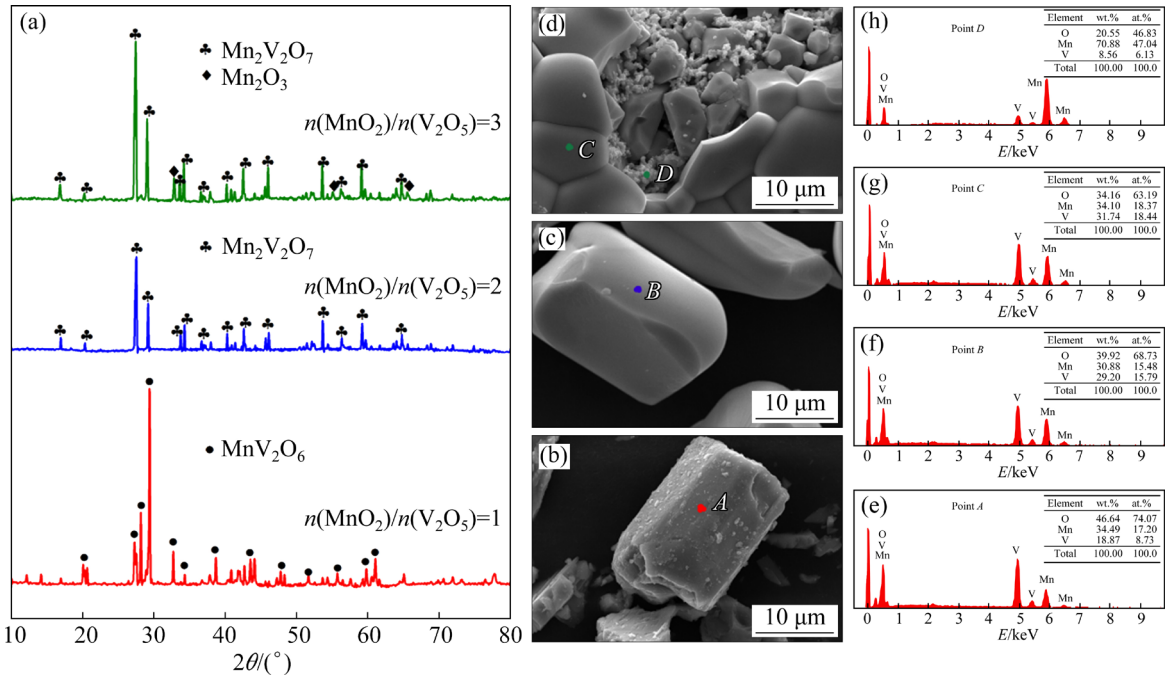


**Fig. 4** XRD patterns (a) and microstructures (b−d) of roasted samples of $MnO_2$−$V_2O_5$ system with different $n(MnO_2)/n(V_2O_5)$ ratios, and corresponding EDS analysis results (e−h): (b) Ratio of 1; (c) Ratio of 2; (d) Ratio of 3

conditions. As indicated in Fig. 4(d), both smooth $Mn_2V_2O_7$ particles and small-sized $Mn_2O_3$ particles were observed. The EDS analyses of Points *C* and *D* confirmed the phase composition with $n(MnO_2)/n(V_2O_5)$ of 3. The reaction equations for $n(MnO_2)/n(V_2O_5)$ ratios of 1, 2 and 3 are depicted in Eqs. (4) to (6).

$$V_2O_5+CaO=CaV_2O_6 \quad (1)$$

$$V_2O_5+2CaO=Ca_2V_2O_7 \quad (2)$$

$$V_2O_5+3CaO=Ca_3V_2O_8 \quad (3)$$

$$2V_2O_5+2MnO_2=2MnV_2O_6+O_2 \quad (4)$$

$$V_2O_5+2MnO_2=Mn_2V_2O_7+O_2 \quad (5)$$

$$4MnO_2=2Mn_2O_3+O_2 \quad (6)$$

### 3.2 Effect of $MnO_2$ addition on $CaO$−$V_2O_5$−$MnO_2$ system

In analyzing the influence of $MnO_2$ on the formation and transformation behavior of vanadates, $MnO_2$ was incrementally added to the $CaO$−$V_2O_5$−$MnO_2$ system with a fixed $n(CaO)/n(V_2O_5)$ ratio of 2. The XRD patterns of the roasted samples are displayed in Fig. 5. The results indicated that, in the absence of $MnO_2$, the only roasting product was $Ca_2V_2O_7$, as previously discussed in Section 3.1. When $MnO_2$ was introduced at a $n(MnO_2)/n(V_2O_5)$ ratio of 1, the intensity of the $Ca_2V_2O_7$ diffraction peaks decreased substantially, and $Mn_2V_2O_7$ appeared in the roasted sample. This suggested that vanadium, which would typically react with CaO, instead combined with $MnO_2$ to form $Mn_2V_2O_7$, as illustrated in Eq. (5). Moreover, the molar ratio of CaO to $V_2O_5$ reacting with CaO exceeded 2 upon the addition of $MnO_2$, leading to the formation of $Ca_3V_2O_8$. Additionally, $Mn_2O_3$, resulting from the decomposition of $MnO_2$, along with excess CaO, was present, indicating that $MnO_2$ decomposed to $Mn_2O_3$ before reacting with $V_2O_5$ during roasting.

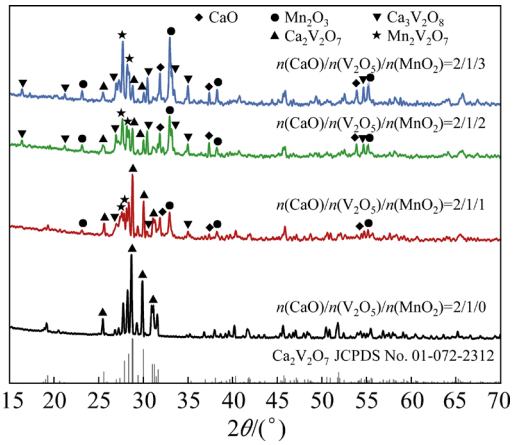


**Fig. 5** XRD patterns of roasted samples of CaO−$V_2O_5$−$MnO_2$ system with different $MnO_2$ additions

As $MnO_2$ addition continued, resulting in $n(MnO_2)/n(V_2O_5)$ ratios of 2 and 3, $Ca_2V_2O_7$ gradually decreased, while $Mn_2V_2O_7$ and $Ca_3V_2O_8$ became the primary vanadates in the roasted material. The residual amounts of CaO and $Mn_2O_3$ also increased. These findings suggested that the addition of $MnO_2$ converted some $Ca_2V_2O_7$ into $Mn_2V_2O_7$, demonstrating a competitive relationship between calcium and manganese in the reaction with vanadium.

Acid leaching experiments were conducted as described in Section 2.3 to quantify the distribution and migration of vanadium in calcium and manganese vanadates during the continuous addition of $MnO_2$. Figure 6 depicts the mass of vanadium in each gram of roasted material. After roasting at 850 °C, all vanadium was present in the form of vanadates. The vanadium content in calcium and manganese vanadates was calculated using the method outlined in Section 2.4. The results indicated that a roasted sample with $n(CaO)/n(V_2O_5)/n(MnO_2)$ of 2/1/0 contained 0.35 g of vanadium per gram of sample, with all vanadium present as $Ca_2V_2O_7$. As $MnO_2$ was gradually added, the total mass of vanadium in 1 g of roasted sample decreased, with vanadium in the form of calcium vanadate also decreasing. Conversely, vanadium in the form of manganese vanadate increased because $MnO_2$ competed for vanadium. Furthermore, the mass ratios of vanadium in calcium and manganese vanadates were calculated and are displayed in Fig. 6. The mass ratios were 3.56, 1.90 and 1.43 when $n(MnO_2)/n(V_2O_5)$ was 1, 2 and 3, respectively. Thus, the mass of vanadium reacting with manganese increases with the addition of $MnO_2$ but remains lower than that reacting with calcium.

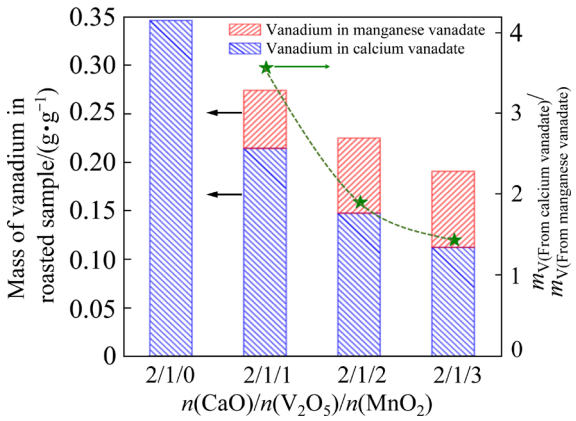


**Fig. 6** Distribution of vanadium in calcium vanadate and manganese vanadate with different $MnO_2$ additions

### 3.3 Effect of CaO addition on $CaO-V_2O_5-MnO_2$ system

The conversion mechanism of manganese vanadate to calcium vanadate was investigated by incrementally adding CaO to the $CaO-V_2O_5-MnO_2$ system with a fixed $n(MnO_2)/n(V_2O_5)$ ratio of 2. The XRD patterns of the roasted samples are shown in Fig. 7. When only $MnO_2$ and $V_2O_5$ were present, the roasting product was $Mn_2V_2O_7$, as discussed in Section 3.1. Upon adding CaO to achieve $n(CaO)/n(V_2O_5)$ ratio of 1, the intensity of the $Mn_2V_2O_7$ diffraction peaks decreased significantly, and $Mn_2O_3$ began to form. The appearance of $Ca_2V_2O_7$ diffraction peaks indicated that some vanadium initially combined with $MnO_2$ had been converted to $Ca_2V_2O_7$ due to the addition of CaO. As CaO addition continued, resulting in an $n(CaO)/n(V_2O_5)$ ratio of 2, the amount of $Mn_2V_2O_7$ decreased, and $Ca_3V_2O_8$ started to form alongside $Ca_2V_2O_7$. This was attributed to the molar ratio of CaO to the actual reacting $V_2O_5$ exceeding 2. Residual CaO and $Mn_2O_3$ were also present. With $n(CaO)/n(V_2O_5)$ ratio of 3, the diffraction peak intensities of both $Ca_2V_2O_7$ and $Mn_2V_2O_7$ decreased significantly, and $Ca_3V_2O_8$ became the primary vanadate in the roasted material. This indicated that, with the progressive addition of CaO, $Mn_2V_2O_7$ and $Ca_2V_2O_7$ were gradually converted to $Ca_3V_2O_8$, highlighting the notable effects of CaO addition on the formation of calcium vanadates.

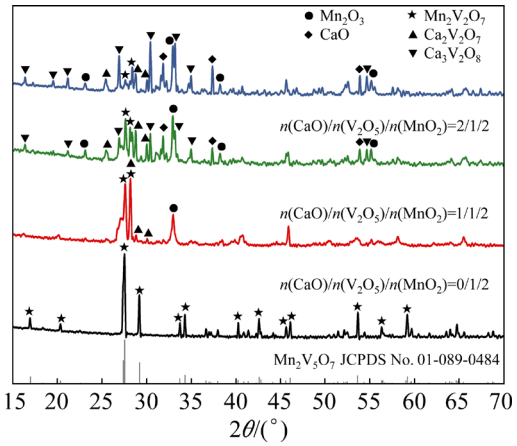


**Fig. 7** XRD patterns of roasted samples of $CaO-V_2O_5-MnO_2$ system with different CaO additions

Figure 8 further illustrates the quantitative characterization results of the effect of CaO addition on vanadate forms. When the $n(CaO)/n(V_2O_5)/n(MnO_2)$ ratio was 0/1/2, the roasted

sample contained 0.32 g of vanadium per gram, all present as $Mn_2V_2O_7$. This value was slightly lower than that for $n(CaO)/n(V_2O_5)/n(MnO_2)$ ratio of 2/1/0, discussed in Section 3.2, due to the relatively higher molecular mass of $Mn_2V_2O_7$ compared to $Ca_2V_2O_7$. At the $n(CaO)/n(V_2O_5)$ ratio of 1, the mass of vanadium in the form of calcium vanadate increased substantially. At ratios of 2 and 3, the amount of vanadium as manganese vanadate gradually decreased, indicating that more vanadium had been converted into calcium vanadate. The green dashed line in Fig. 8 represents the mass ratios of vanadium in calcium and manganese vanadates. The values are 0.67, 1.90, and 3.69 for $n(CaO)/n(V_2O_5)$ ratios of 1, 2, and 3, respectively, indicating that more vanadium reacts with calcium as CaO is added. However, the mass of vanadium reacting with manganese decreased, suggesting that calcium's reactivity with vanadium is higher than that of manganese.

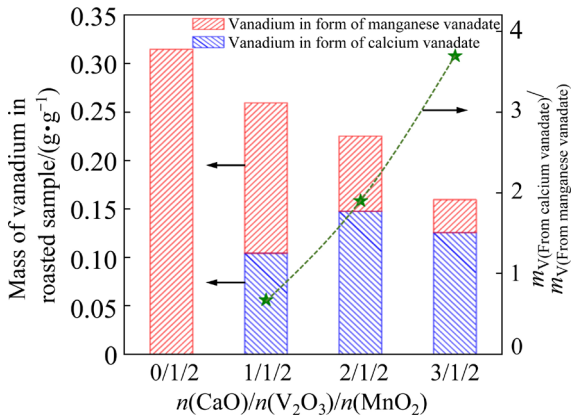


**Fig. 8** Distribution of vanadium in calcium vanadate and manganese vanadate with different CaO additions

### 3.4 Effect of $n(CaO)/n(V_2O_5)$ and $n(MnO_2)/n(V_2O_5)$ on $CaO−V_2O_5−MnO_2$ system

In the study of the effects of $n(CaO)/n(V_2O_5)$ and $n(MnO_2)/n(V_2O_5)$ on the $CaO−V_2O_5−MnO_2$ system, the mass of $V_2O_5$ in the system was kept constant while CaO and $MnO_2$ were incrementally added at fixed ratios of $n(CaO)/n(V_2O_5)$ and $n(MnO_2)/n(V_2O_5)$. Figure 9 displays the XRD patterns of roasted samples under various conditions. When $n(CaO)/n(V_2O_5)/n(MnO_2)$ was 1/2/1, $CaV_2O_6$ emerged as the dominant phase in the roasted sample. Only a small portion of vanadium reacted with manganese to form $Mn_2V_2O_7$, with most manganese existing as $Mn_2O_3$. This indicated that under these conditions, vanadium's affinity for calcium surpassed its affinity for manganese, resulting in the predominance of $CaV_2O_6$. At $n(CaO)/n(V_2O_5)/n(MnO_2)$ of 1/1/1, the intensity of the $CaV_2O_6$ diffraction peak significantly decreased, and $Mn_2V_2O_7$ became more prominent. When $n(CaO)/n(V_2O_5)/n(MnO_2)$ was 3/2/3, the $CaV_2O_6$ diffraction peaks vanished completely, and $Ca_2V_2O_7$ formed. This transformation indicated that continuous addition of CaO converted $CaV_2O_6$ into $Ca_2V_2O_7$, while manganese vanadate remained as $Mn_2V_2O_7$. At $n(CaO)/n(V_2O_5)/n(MnO_2)$ of 2/1/2, $Ca_2V_2O_7$ further converted into $Ca_3V_2O_8$. When $n(CaO)/n(V_2O_5)/n(MnO_2)$ was 3/1/3, the phase composition resembled that at 2/1/2, but with strengthened $Ca_3V_2O_8$ diffraction peaks and weakened $Ca_2V_2O_7$ peaks.

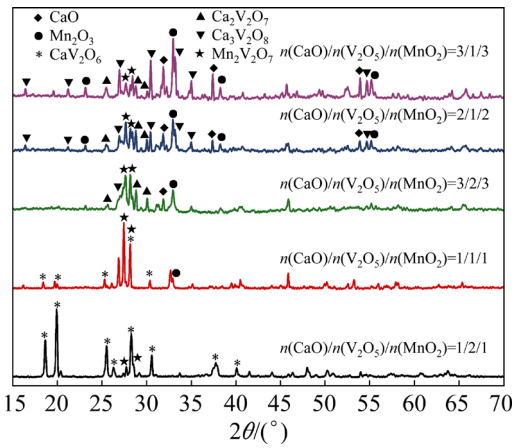


**Fig. 9** XRD patterns of roasted samples of $CaO−V_2O_5−MnO_2$ system with different CaO and $MnO_2$ additions

$MnV_2O_6$ was formed in the $MnO_2−V_2O_5$ two-phase system, whereas manganese vanadate was present as $Mn_2V_2O_7$ throughout the $CaO−V_2O_5−MnO_2$ three-phase system. This disparity can be attributed to the interaction of $V_2O_5$ with CaO, leaving $MnO_2$ in excess relative to $V_2O_5$ available for reaction. This absence of conditions necessary for $MnV_2O_6$ formation underscored vanadium's stronger affinity for calcium over manganese.

Figure 10 shows the competitive relationship between CaO and $MnO_2$ across different $n(CaO)/n(V_2O_5)/n(MnO_2)$ ratios through quantitative vanadate characterization. Results indicated that at $n(CaO)/n(V_2O_5)/n(MnO_2)$ of 1/2/1, 0.42 g of vanadium was contained in 1 g of roasted sample, with 0.35 g as calcium vanadate and only 0.07 g as manganese vanadate, consistent with XRD patterns

in Fig. 9. At this ratio, the mass ratio of vanadium present as calcium vanadate to manganese vanadate reached a maximum of 5.20. Upon increasing $n(CaO)/n(V_2O_5)$ and $n(MnO_2)/n(V_2O_5)$ to achieve $n(CaO)/n(V_2O_5)/n(MnO_2)$ of 1/1/1, the mass of vanadium in manganese vanadate increased substantially, nearly equalizing with that of calcium vanadate. Continued addition of CaO and $MnO_2$ to achieve ratios of 1.5 and 2 led to a decrease in vanadium mass as manganese vanadate, consistently less than calcium vanadate. Particularly at $n(CaO)/n(V_2O_5)/n(MnO_2)$ of 3/1/3, the abundant CaO provided favorable kinetic conditions for vanadium calcification, resulting in a vanadium mass 4.80 times greater in calcium vanadate than that that in manganese vanadate. These findings highlighted that $n(CaO)/n(V_2O_5)/n(MnO_2)$ of 1/1/1 optimally favors manganese vanadate generation, while calcium vanadate remains the predominant form in the system.

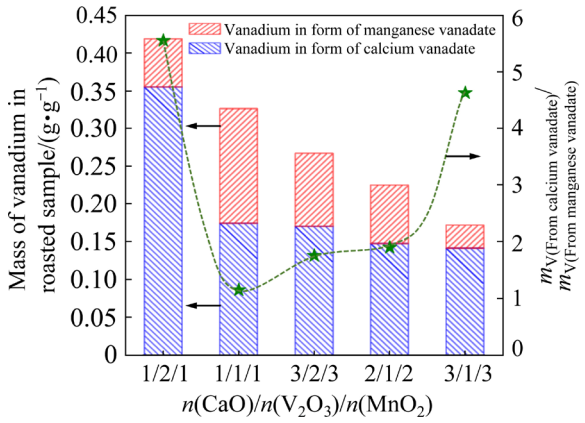


**Fig. 10** Distribution of vanadium in calcium vanadate and manganese vanadate with different CaO and $MnO_2$ additions

### 3.5 Effect of roasting temperature on CaO−$V_2O_5$−$MnO_2$ system

In addition to varying $n(CaO)/n(V_2O_5)/n(MnO_2)$, roasting temperature significantly influenced the generation and conversion of vanadates in this study. The XRD patterns of samples roasted with $n(CaO)/n(V_2O_5)/n(MnO_2)$ of 2/1/2 at different temperatures are illustrated in Fig. 11. At 350 and 450 °C, $V_2O_5$ and CaO remained unchanged, with no vanadate phases detected in the roasted samples. Additionally, $Mn_3O_4$ diffraction peaks appeared alongside $MnO_2$, resulting from $MnO_2$ decomposition, indicating difficulty in vanadate formation at lower roasting temperatures. Upon increasing the roasting temperature to 550 °C, the intensity of $V_2O_5$ diffraction peaks significantly decreased, $Mn_2V_2O_7$ formed, and $Mn_3O_4$ further decomposed into $Mn_2O_3$, consistent with decomposition process of $MnO_2$. At 650 °C, $V_2O_5$ diffraction peaks became difficult to detect, indicating complete conversion of $V_2O_5$ into vanadate. In the roasted sample, $CaV_2O_6$, $Ca_2V_2O_7$ and $Mn_2V_2O_7$ coexisted. At 750 °C, $CaV_2O_6$ diffraction peaks were barely observed, with calcium vanadate primarily in the form of $Ca_2V_2O_7$ and manganese vanadate as $Mn_2V_2O_7$. Increasing the roasting temperature to 850 °C resulted in $Ca_2V_2O_7$ converting into $Ca_3V_2O_8$, accompanied by a significant decrease in CaO diffraction peak intensity. This indicated that the type of calcium vanadate was influenced not only by CaO addition but also by roasting temperature. Sequential generation of $CaV_2O_6$, $Ca_2V_2O_7$ and $Ca_3V_2O_8$ occurred with increasing roasting temperature, while manganese vanadate remained consistently as $Mn_2V_2O_7$. At 950 °C, diffraction peaks of calcium vanadate and manganese vanadate were undetectable, with $Ca_{2.6}Mn_{1.9}V_3O_{12}$ being the main phase in the roasted sample.

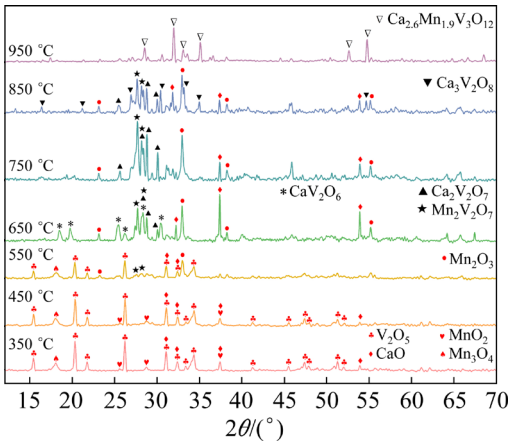


**Fig. 11** XRD patterns of roasted samples of CaO−$V_2O_5$−$MnO_2$ system at different roasting temperatures

Figure 12 shows the quantitative characterization of calcium vanadate and manganese vanadate in samples roasted from 650 to 850 °C indicating interference from $V_2O_5$ at 350, 450 and 550 °C that hindered the mass calculation of vanadate. At 950 °C, both calcium and manganese were incorporated into a single phase, $Ca_{2.6}Mn_{1.9}V_3O_{12}$, making it challenging to quantitatively characterize vanadium distribution between calcium vanadate

and manganese vanadate under these conditions. Despite sequential production of $CaV_2O_6$, $Ca_2V_2O_7$ and $Ca_3V_2O_8$, there was no significant difference in vanadium distribution between calcium vanadate and manganese vanadate in the range of 650−850 °C. The mass ratio of vanadium present as calcium vanadate to manganese vanadate consistently remained equal to approximately 2.

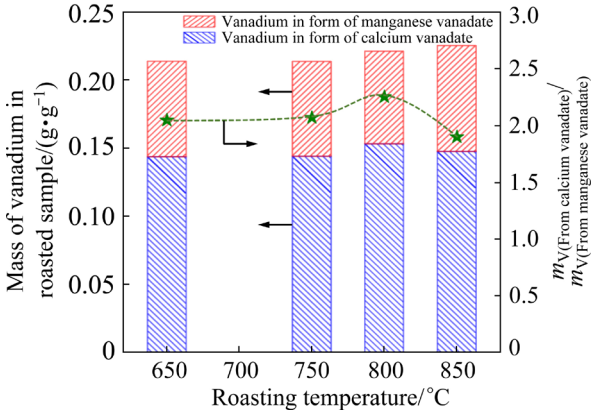


**Fig. 12** Distribution of vanadium in calcium vanadate and manganese vanadate at different temperatures

## 4 Evaluation

Based on the above findings, the effects of $n(CaO)/n(V_2O_5)/n(MnO_2)$ and roasting temperature on the phase evolution of vanadate and the distribution of vanadium were determined. Furthermore, Fig. 13 compares the advantages of CaO roasting versus $MnO_2$ roasting in vanadium extraction. This comparison integrates current research on calcification roasting and manganese roasting processes for vanadium slag and chromium-containing vanadium slag.

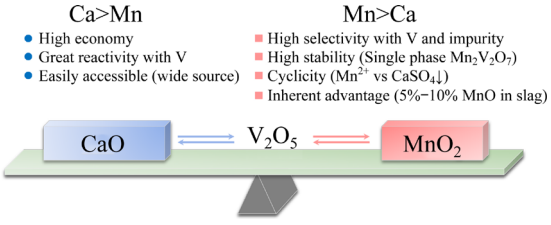


**Fig. 13** Advantages of CaO roasting and $MnO_2$ roasting in vanadium extraction

Vanadium exhibited slightly stronger reactivity with CaO compared to $MnO_2$. In our experiments, when both $n(CaO)/n(V_2O_5)$ and $n(MnO_2)/n(V_2O_5)$ were set as 2, the mass of vanadium reacted with CaO was twice that reacted with $MnO_2$. Additionally, our group [34] demonstrated that the diffusion product thickness of the $CaO-V_2O_5$ couple exceeded that of the $MnO_2-V_2O_5$ couple under identical roasting times. Moreover, CaO was more cost-effective and readily available compared to $MnO_2$, making it more versatile for the calcification roasting processes of vanadium slag and chromium-containing vanadium slag in the future.

In contrast, $MnO_2$ exhibited weaker reactivity with vanadium than CaO, suggesting that $MnO_2$ is selectively responsive to vanadium. This conclusion is supported by the separation behavior of vanadium and chromium during manganese roasting of chromium-containing vanadium slag. Unlike the sequential production of $CaV_2O_6$, $Ca_2V_2O_7$ and $Ca_3V_2O_8$ in the calcium−vanadium reaction, vanadium−manganese reaction products are more stable. Manganese vanadate in roasted samples consistently existed as $Mn_2V_2O_7$, which did not transform into water-insoluble sulfate during acid leaching, enabling the recycling of manganese ions. Furthermore, an advantageous aspect was the presence of 5% to 10% MnO derived from vanadium−titanium magnetite in vanadium slag, which contributed to vanadium conversion and reduced the need for calcium additives.

In conclusion, both CaO and $MnO_2$ offered distinct advantages in the vanadium extraction process. Leveraging their synergistic effects to enhance vanadium extraction from vanadium slag and chromium-containing vanadium slag constitutes a focal point for our future research.

## 5 Conclusions

(1) In the $CaO-V_2O_5$ system, $CaV_2O_6$ and $Ca_2V_2O_7$ were generated sequentially when $n(CaO)/n(V_2O_5)$ was 1 and 2. When $n(CaO)/n(V_2O_5)$ was 3, $Ca_2V_2O_7$ and $Ca_3V_2O_8$ coexisted. In the $MnO_2-V_2O_5$ system, $MnV_2O_6$ and $Mn_2V_2O_7$ formed when $n(MnO_2)/n(V_2O_5)$ was 1 and 2. $Mn_2V_2O_7$ and $Mn_2O_3$ coexisted when $n(MnO_2)/n(V_2O_5)$ was 3.

(2) When $MnO_2$ was gradually added to the $CaO-V_2O_5-MnO_2$ system with $n(CaO)/n(V_2O_5)$ of 2, some $Ca_2V_2O_7$ converted to $Mn_2V_2O_7$. Conversely, when CaO was gradually added to the $CaO-V_2O_5-MnO_2$ system with $n(MnO_2)/n(V_2O_5)$ of 2, some $Mn_2V_2O_7$ converted to $Ca_2V_2O_7$ and $Ca_3V_2O_8$. This indicates that vanadium had a higher

binding affinity with calcium than that with manganese. When $n(CaO)/n(V_2O_5)/n(MnO_2)$ was 1/1/1, the mass of vanadium present as calcium vanadate was nearly equal to that present as manganese vanadate.

(3) At $n(CaO)/n(V_2O_5)/n(MnO_2)$ of 2/1/2, vanadate formation began after 550 °C, with $MnO_2$ decomposing gradually to form $Mn_3O_4$ and $Mn_2O_3$. After 650 °C, $CaV_2O_6$, $Ca_2V_2O_7$ and $Ca_3V_2O_8$ generated sequentially, while manganese vanadate remained in the form of $Mn_2V_2O_7$. The impact of roasting temperature on the conversion of calcium vanadate and manganese vanadate was minimal. When the roasting temperature ranged from 650 to 850 °C, the mass ratio of vanadium present as calcium vanadate to manganese vanadate remained stable at approximately 2.

## CRediT authorship contribution statement

**Jing WEN:** Conceptualization, Writing − Original draft, Writing – Review & editing, Investigation, Visualization; **Tao JIANG:** Conceptualization, Writing − Original draft, Writing – Review & editing, Visualization, Resources; **Fei-fei LI:** Investigation, Validation; **Tang-xia YU:** Investigation, Writing – Review & editing; **Bo-jian CHEN:** Investigation.

## Declaration of competing interest

The authors declare that they have no known competing financial interests or personal relationships that could have appeared to influence the work reported in this paper.

## Acknowledgments

This work was finally supported by the National Natural Science Foundation of China (Nos. 52204309, 52174277, 52374300).

## References

[1] LEE J C, KURNIAWAN, KIM E Y, CHUNG K W, KIM R, JEON H S. A review on the metallurgical recycling of vanadium from slags: Towards a sustainable vanadium production [J]. Journal of Materials Research and Technology, 2021, 12: 343−364.

[2] AN Ya-rui, MA Bao-zhong, LI Xiang, CHEN Yong-qiang, WANG Cheng-yan, WANG Bao-hua, GAO Ming-lei, FENG Guo-sheng. A review on the roasting-assisted leaching and recovery of V from vanadium slag [J]. Process Safety and Environmental Protection, 2023, 173: 263−276.

[3] WANG Zheng-hao, CHEN Liang, QIN Zhi-feng, YANG Ke, LIANG Bin, ZHANG Guo-quan, LIU Chang-jun, LUO Dong-mei. A green and efficient route for simultaneous recovery of low valence of vanadium and chromium, titanium and iron from vanadium slag [J]. Resources, Conservation and Recycling, 2022, 178: 106046.

[4] DIAO Jiang, QIAO Yong, ZHANG Xie, JI Cheng-qing, XIE Bing. Growth mechanisms of spinel crystals in vanadium slag under different heat treatment conditions [J]. CrystEngComm, 2015, 17: 7300−7305.

[5] SUN Shi-bo, FANG Li-wei, GUO Hui, SUN Li-ping, LIU Yong, CHENG Yuan-hui. A bifunctional liquid fuel cell coupling power generation and $V^{3.5+}$ electrolytes production for all vanadium flow batteries [J]. Advanced Science, 2023, 10: 2207728.

[6] ZHOU An-hui, QIU Zhao-fu, YANG Ji, YAN Rui-qi. A magnetic chitosan for efficient adsorption of vanadium(V) from aqueous solution [J]. Environmental Science and Pollution Research, 2022, 29: 76263−76274.

[7] WANG Jin, ZHANG Pan, WANG Shao-dong, YANG Lin, LUO Jian-hong, HE Wen-yi, DU Guang-chao, WANG Xin-long, ZHANG Zhi-ye, YANG Xiu-shan. Evaluation of a green-sustainable industrialized cleaner production for FeV50 and FeV80 alloys from vanadium slag by calcification roasting–ammonia on-line cycle [J]. Journal of Cleaner Production, 2021, 320: 128896.

[8] ALAZMI A, WAN C T, COSTA P M F J, BRUSHETT F R. Exploration of reduced graphene oxide microparticles as electrocatalytic materials in vanadium redox flow batteries [J]. Journal of Energy Storage, 2022, 50: 104192.

[9] WANG Ming-ming, GAO Xiu-hua, SONG Li-ying, ZHU Cheng-lin, MISRA R D K, DU Lin-xiu. Microstructure-toughness relationship in the simulated CGHAZ of V−N microalloyed X80 pipeline steel [J]. Materials Science and Technology, 2021, 37: 1047−1059.

[10] NI Guo-long, ZHAO Ding-guo, WANG Shu-huan, SONG Chun-yan. Investigation of V−N micro-alloying using nitrogen bottom blowing [J]. Transactions of the Indian Institute of Metals, 2020, 73: 2693−2701.

[11] WANG Shuai, GUO Yu-feng, ZHENG Fu-qiang, CHEN Feng, YANG Ling-zhi, JIANG Tao, QIU Guan-zhou. Behavior of vanadium during reduction and smelting of vanadium titanomagnetite metallized pellets [J]. Transactions of Nonferrous Metals Society of China, 2020, 30: 1687−1696.

[12] XIANG Jun-yi, HUANG Qing-yun, LV Xue-wei, BAI Chen-guang. Multistage utilization process for the gradient-recovery of V, Fe, and Ti from vanadium-bearing converter slag [J]. Journal of Hazardous Materials, 2017, 336: 1−7.

[13] JIANG Tao, WEN Jing, ZHOU Mi, XUE Xiang-xin. Phase evolutions, microstructure and reaction mechanism during calcification roasting of high chromium vanadium slag [J]. Journal of Alloys and Compounds, 2018, 742: 402−412.

[14] WEN Jing, JIANG Tao, LIU Ya-jing, XUE Xiang-xin. Extraction behavior of vanadium and chromium by calcification roasting-acid leaching from high chromium vanadium slag: Optimization using response surface methodology [J]. Mineral Processing and Extractive

Metallurgy Review, 2019, 40: 56−66.

[15] YUAN Shuai, QIN Yong-hong, JIN Yong-peng, LI Yan-jun. Improving vanadium extraction from refractory stone coal by suspension roasting [J]. Transactions of Nonferrous Metals Society of China, 2023, 33: 902−916.

[16] TENG Qing, YANG Zhi-chao, WANG Hong-jun. Recovery of vanadium and nickel from spent-residue oil hydrotreating catalyst by direct acid leaching-solvent extraction [J]. Transactions of Nonferrous Metals Society of China, 2023, 33: 325−336.

[17] ZENG Li, LI Qing-gang, XIAO Lian-sheng. Extraction of vanadium from the leach solution of stone coal using ion exchange resin [J]. Hydrometallurgy, 2009, 97: 194−197.

[18] WEN Jia-wei, WANG Xue-li, YU Feng-shan, TIAN Mao-lin, WANG Chun-xia, HUANG Guo-yong, XU Sheng-ming. Recovery and value-added utilization of critical metals from spent catalysts for new energy industry [J]. Journal of Cleaner Production, 2023, 419: 138295.

[19] MA Li-wen, XI Xiao-li, CHEN Jia-peng, GUO Fan, YANG Zi-jie, NIE Zuo-ren. Comprehensive recovery of W, V, and Ti from spent selective reduction catalysts [J]. Rare Metals, 2023, 42: 3518−3531.

[20] YU Tang-xia, JIANG Tao, WEN Jing, SUN Hong-yan, LI Ming, PENG Yi. Effect of chemical composition on the element distribution, phase composition and calcification roasting process of vanadium slag [J]. International Journal of Minerals, Metallurgy and Materials, 2022, 29: 2144−2151.

[21] WEN Jing, JIANG Tao, YU Tang-xia, CHEN Bo-jian, LI Lin. Clean and efficient extraction of vanadium from vanadium slag: Effect of manganese on the phase composition and vanadium extraction process [J]. Journal of Cleaner Production, 2022, 367: 133077.

[22] DONG Zi-hui, ZHANG Jie, YAN Bai-jun. A new approach for the comprehensive utilization of vanadium slag [J]. Metallurgical and Materials Transactions B, 2022, 53: 2198−2208.

[23] DONG Zi-hui, ZHANG Jie, YAN Bai-jun. Co-extraction of vanadium titanium and chromium from vanadium slag by oxalic acid hydrothermal leaching with synergy of Fe powder [J]. Metallurgical and Materials Transactions B, 2021, 52: 3961−3969.

[24] WEN Jing, JIANG Tao, SUN Hong-yan, YU Tang-xia. Novel understanding of simultaneous extraction of vanadium and manganese from vanadium slag and low-grade pyrolusite based on selective oxidation–reduction roasting [J]. ACS Sustainable Chemistry & Engineering, 2020, 8: 5927−5936.

[25] GUO Yun, LI Hong-yi, YUAN Yi-heng, HUANG Jie, DIAO Jiang, LI Gang, XIE Bing. Microemulsion leaching of vanadium from sodium-roasted vanadium slag by fusion of leaching and extraction processes [J]. International Journal of Minerals, Metallurgy and Materials, 2021, 28: 974−980.

[26] XIANG Jun-yi, LUO Ming-shuai, LU Xi, BAI Lu-wei, ZHU Zhong-peng, HUANG Qing-yun, ZHANG Sheng-qin, GUO Kun-peng, LV Xue-wei. Recovery of vanadium from vanadium slag by composite additive roasting–acid leaching process [J]. Journal of Iron and Steel Research International, 2023, 30: 1426−1439.

[27] XIANG Jun-yi, BAI Lu-wei, LU Xi, LUO Ming-shuai, HUANG Qing-yun, ZHANG Sheng-qin, LV Xue-wei. Selective recovery of vanadium from high-chromium vanadium slag by a mechanically activated low-sodium salt roasting−water leaching process [J]. Journal of Environmental Chemical Engineering, 2023, 11: 111304.

[28] ZHANG Ju-hua, ZHANG Wei, XUE Zheng-liang. Oxidation kinetics of vanadium slag roasting in the presence of calcium oxide [J]. Mineral Processing and Extractive Metallurgy Review, 2017, 38: 265−273.

[29] WEN Jing, JIANG Tao, XU Ying-zhe, CAO Jing, XUE Xiang-xin. Efficient extraction and separation of vanadium and chromium in high chromium vanadium slag by sodium salt roasting−$(NH_4)_2SO_4$ leaching [J]. Journal of Industrial and Engineering Chemistry, 2019, 71: 327−335.

[30] FU Zi-bi, JIANG Lin, LI Ming, WU Zen-xiu. Simultaneous extraction of vanadium and chromium from vanadium chromium slag by sodium roasting [J]. Iron Steel Vanadium Titanium, 2020, 41: 1−6.

[31] LI Hong-yi, WANG Cheng-jie, LIN Min-min, GUO Yun, XIE Bing. Green one-step roasting method for efficient extraction of vanadium and chromium from vanadium−chromium slag [J]. Powder Technology, 2020, 360: 503−508.

[32] LIU Biao, DU Hao, WANG Shao-na, ZHANG Yi, ZHENG Shi-li, LI Lan-jie, CHEN Dong-hui. A novel method to extract vanadium and chromium from vanadium slag using molten NaOH−$NaNO_3$ binary system [J]. AIChE Journal, 2013, 59: 541−552.

[33] LIU Shi-yuan, XUE Wei-hua, WANG Li-jun. Extraction of the rare element vanadium from vanadium-containing materials by chlorination method: A critical review [J]. Metals, 2021, 11: 1301.

[34] WEN Jing, SUN Hong-yan, JIANG Tao, CHEN Bo-jian, LI Fang-fang, LIU Meng-xia. Comparison of interface reaction behaviors of CaO−$V_2O_5$ and $MnO_2$−$V_2O_5$ solid-state systems based on diffusion couple method [J]. International Journal of Minerals, Metallurgy and Materials, 2023, 30: 834−843.

[35] WEN Jing, JIANG Tao, SUN Hong-yan, YU Tang-xia, LI Ming, PENG Yi. Investigation on separation principle of vanadium and chromium among $Fe_2VO_4$−CaO−$FeCr_2O_4$ system: Simplify and simulate calcification roasting process of vanadium−chromium slag [J]. Journal of Industrial and Engineering Chemistry, 2022, 115: 378−389.

[36] WEN Jing, JIANG Tao, WANG Jun-peng, LU Long-gang, SUN Hong-yan. Cleaner extraction of vanadium from vanadium−chromium slag based on $MnO_2$ roasting and manganese recycle [J]. Journal of Cleaner Production, 2020, 261: 121205.

[37] WEN Jing, JIANG Tao, WANG Jun-peng, GAO Hui-yang, LU Long-gang. An efficient utilization of high chromium vanadium slag: Extraction of vanadium based on manganese carbonate roasting and detoxification processing of chromium-containing tailings [J]. Journal of Hazardous Materials, 2019, 378: 120733.

[38] ZHANG X, XIE B, DIAO J, LI X J. Nucleation and growth kinetics of spinel crystals in vanadium slag [J]. Ironmaking & Steelmaking, 2012, 39: 147−154.
[39] LI Hong-yi, FANG Hai-xing, WANG Kang, ZHOU Wang, YANG Zhao, YAN Xiao-man, GE Wen-sun, LI Qian-wen, XIE Bing. Asynchronous extraction of vanadium and chromium from vanadium slag by stepwise sodium roasting−water leaching [J]. Hydrometallurgy, 2015, 156: 124−135.

# 钒渣钙化焙烧 $CaO-V_2O_5-MnO_2$ 体系中钒酸钙和钒酸锰的转化机制

温 婧[1]，姜 涛[1,2,3]，李菲菲[1]，余唐霞[1]，陈泊键[1]

1. 东北大学 冶金学院，沈阳 110819；
2. 东北大学 多金属共生矿生态化冶金教育部重点实验室，沈阳 110819；
3. 辽宁省冶金传感器材料及技术重点实验室，沈阳 110819

**摘 要**：基于钒渣的钙化焙烧过程建立了 $CaO-V_2O_5-MnO_2$ 简化体系，对该体系焙烧过程中钒酸盐的转化行为进行了定性和定量研究。结果表明，随着体系中组元配比 $n(CaO)/n(V_2O_5)/n(MnO_2)$和焙烧温度的变化，钒酸钙和钒酸锰会相互转化。在 $n(CaO)/n(V_2O_5)$为 2 的条件下不断加入 $MnO_2$，部分 $Ca_2V_2O_7$ 会转化为 $Mn_2V_2O_7$。以钒酸钙形式存在的钒的质量总是大于以钒酸锰形式存在的钒。相反，$n(MnO_2)/n(V_2O_5)$为 2 的条件下不断加入 CaO，$Mn_2V_2O_7$ 逐渐转化为 $Ca_2V_2O_7$ 和 $Ca_3V_2O_8$，钒与钙的结合能力高于钒与锰的结合能力。焙烧产物中钒酸钙的种类受组元配比 $n(CaO)/n(V_2O_5)/n(MnO_2)$和焙烧温度的影响，钒酸锰总是以 $Mn_2V_2O_7$ 形式存在。钒酸钙和钒酸锰的转化受焙烧温度影响较小。在 $n(CaO)/n(V_2O_5)/n(MnO_2)$为 2/1/2、焙烧温度为 650~850 ℃时，以钒酸钙和钒酸锰形式存在的钒的质量比接近 2。

**关键词**：转化机制；$CaO-V_2O_5-MnO_2$；钒酸钙；钒酸锰；钒渣；钙化焙烧

**(Edited by Xiang-qun LI)**